Research Article

Wireless Passive High-Temperature Sensor Readout System for Rotational-Speed Measurement

Yingping Hong,[1,2] **Pengyu Jia,**[1,2] **Xihao Guan,**[1] **Jijun Xiong,**[1] **Wenyi Liu,**[1] **Huixin Zhang,**[1] **and Chen Li** [1,2]

[1]*Science and Technology on Electronic Test and Measurement Laboratory, Taiyuan 030051, China*
[2]*Key Laboratory of Instrumentation Science and Dynamic Measurement, Ministry of Education, North University of China, Taiyuan 030051, China*

Correspondence should be addressed to Chen Li; lichen@nuc.edu.cn

Rotational-speed measurement in harsh environments is an important topic. However, the high rotation results in rapid frequency variations in the signals of a sensor and changes in physical properties under extreme thermal circumstances cause significant difficulties in reading signals. To address this problem, we adopt wireless passive measurement methods to design a special characteristic signal circuit module that achieves precise measurement of rotational speed at high temperatures. The sensor and the readout system include a variable frequency source, a readout antenna, and a radio frequency demodulation circuit. Herein, a demodulation detector of the signal conversion circuit is designed and used in the envelope detection module of the single sideband demodulation method. In addition, a conversion circuit test platform for high-temperature environment sensor signal is developed. From the testing, the output signal demodulation of the sensor was observed under a maximum temperature of 700°C with error less than 0.12%. The new sensor and measurement method do not require physical leads and achieve wireless noncontact accurate measurement of rotational speed at high temperature.

1. Introduction

Rotational-speed sensors are widely used in aerospace, industrial control, traffic, and other fields, and the speed parameters in high-temperature environments are key for evaluating the working conditions of aero engines, space rocket engines, and ultra-high-speed turbo pumps [1–5]. However, the inability to obtain real-time and in situ information on the working state parameters such as the rotational speed of significant rotating components at high temperatures significantly affects the performance improvement of rotational speed devices in harsh environments. Consequently, there are several studies on related speed sensors.

Giebeler et al. proposed a magnetic rotational sensors based on giant magnetoresistance (GMR) effect that were reliable at temperatures exceeding 170°C [6]. However, magnetic materials degauss at high temperatures; therefore,

GMR sensor is not suitable for high-temperature application. Huang et al. proposed that attaching two layers of hysteresis switches to count pulses, and angular speed can enable measurement with low uncertainties [7]. Li et al. designed a predetermined material stuck on the rotational shaft as an electrostatic sensor to measure rotational speed [8]. Tani et al. proposed a tribocharge sensor with a PTFE film. The film is charged by segmented electrodes, and the sensor can record approximately 2000 rpm [9]. Although the sensors have high dynamic response capability in high-speed measurement, in the low-speed area owing to the unstable electric charge, the time response is unsatisfactory, so it is not widely used. Lin and Ding proposed a method that measures the rotational speed of the engine from the lowest harmonic frequency component of its vibration signals [10]. Although this measurement method is simple and accurate, its high-temperature application is restricted.

Because noncontact detection of rotor rotating is feasible, imaging methods can be used to measure rotational speed. Kędzierski proposed a rotational-speed measurement calibration based on high-speed imaging [11]. The uncertainty of the method was calculated and tested with turbo-engines. Wang et al. [12] proposed that the rotational speed can be measured by a low-cost digital imaging device. Autocorrelation algorithms can calculate the rotational speed based the image without a marker on the rotor; although the measurement method has advantages such as noncontact measurement and high accuracy, its stability in harsh environments is limited. In addition, Gintner proposed a rotational-speed sensor with a soft magnetic core and a resonant circuit that operate up to 200°C and measures ranges of the sensor covers from static status to high speed [13]. Li et al. proposed sensors based on low temperature cofired ceramic (LTCC) [14]. Although the two sensors can operate in high-temperature environment, their dynamic response is unsatisfactory and cannot be used for precise measurement of rotational speed. For sensor readout system, vector network analyzers (VNAs) are widely used [15, 16]. In 2009, Nopper et al. presented a readout system for wireless passive sensors based on LC resonant circuits [17]. The system includes a coil as readout antenna, an LC resonator as sensor, an analog frontend, and a digital signal-processing unit. The analog frontend generates a frequency-variable signal to enable the digital signal-processing unit to detect the equivalent impedance of the readout coil. However, the sweep time limits high-speed sensing and the size of VNA, hindering its applicability. Moreover, wireless passives are also widely used in measurement. Several passive RFID sensors for temperature have been proposed. Wang et al. proposed temperature sense tag based on UHF RFID that can measure up to 120°C. UHF RFID is passive and has high sensitivity. Nonetheless, the current leaks across the PN-junctions with exponential growth at high temperatures and the chips cannot function [18]. The angle of the antenna pair affects the antenna gain and uncertainty [19].

To accurately measure the rotational speed in a high-temperature environment whereas ensuring a significant response speed and stability of the sensor, we propose a wireless passive sensor with square coils and parallel capacitors manufactured using thick film integration technology and corresponding data readout system. The readout system consists of a radio frequency (RF), signal generator, a readout antenna, and a directional coupler. Consequently, the fabricated rotational-speed sensor is suitable for high-temperature applications, and the readout system fulfils the requirement of responding to rapidly changing signals in high rotational speed sensing applications, such as rotational speed detection.

2. Sensor Principle

2.1. Circuit Equipment Model.
As shown in Figure 1, the RF signal generating subsystem generates stimulus with variable frequency. For the rotor rotating, the lateral displacement between the sensor coil and the readout antenna changes periodically. Therefore, the rotational speed can be mea-

sured by detecting the coupling coefficient. The RF signal subsystem and directional coupler are 50Ω systems. The equipment impendence depends on input frequency and coupled coefficient. The impendence of readout antenna is

$$\underline{Z} = R_r + j\omega L_r + \frac{\omega^2 M^2}{R_s + j\omega L_s + (1/j\omega C_s)}, \tag{1}$$

where R_r is the series resistance of readout antenna, $\omega = 2\pi f$ is the angular frequency, and M is the mutual inductance between the readout antenna and sensor inductor. For the 50Ω source, the reflection coefficient Γ is

$$\Gamma = \left(\frac{\underline{Z} - Z_s}{\underline{Z} + Z_s}\right)\bigg|_{Z_s=50\Omega}. \tag{2}$$

If $\underline{Z} > 50\Omega$, the reflection coefficient Γ can be written as a

$$\Gamma = 1\frac{100}{\underline{Z} + 50}. \tag{3}$$

The directional coupler is a 3-port coupler and is connected reversely. The RF signal generator relates to transmitted port, and the readout antenna is connected to the input port. The reflection coefficient and Z are displayed in Figure 2.

Figure 2 shows the local minimum peak of reflection coefficient at a frequency slightly larger than the resonance frequency. The output of the directional coupler coupled terminal is

$$V_{cp} = C_{3,1}\Gamma = C_{3,1}\left(1 - \frac{100}{50 + R_r + j\omega L_r + \left(\omega^2 M^2/R_s + j\omega L_s(1/j\omega C_s)\right)}\right), \tag{4}$$

where $C_{3,1}$ is the coupling factor of directional coupler from the input port to the coupled port.

2.2. Sensor Rotating Model.
The readout antenna measures coupling coefficient k to quantify the strength of the inductive coupling between the sensor and readout antenna. The coupling coefficient k describes the lateral displacement between the sensor and antenna. Using a high-temperature glue, the sensor was mounted on the motor. Therefore, the rotor and the lateral displacement between the sensor and antenna have a periodic variation of the same frequency in phase. The square coils are more useful and efficient compared to round coils [20]. Therefore, we use square coils with outmost turn $l_0 = 40\,mm$ as readout antenna and sensor coils. Figure 3 shows a plot of the coupling coefficient k versus the lateral displacement between the sensor and the antenna.

From the simulation, the sensor S_{11} parameter is the smallest at 132 MHz, and $S_{11} = -9.79\,dB$. Therefore, in the speed parameter test, the frequency at the lowest value of S_{11} is selected as the excitation source frequency value. The

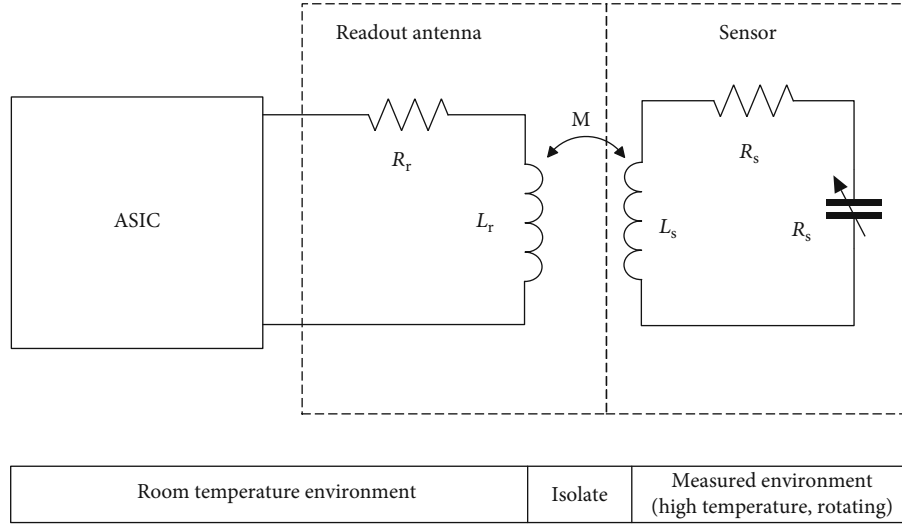| Room temperature environment | Isolate | Measured environment (high temperature, rotating) |

FIGURE 1: Schematic of the rotational-speed sensor system. The sensor circuit is inductively coupled to the readout antenna. The RF generator generates several frequency signal and detects the coupling coefficient.
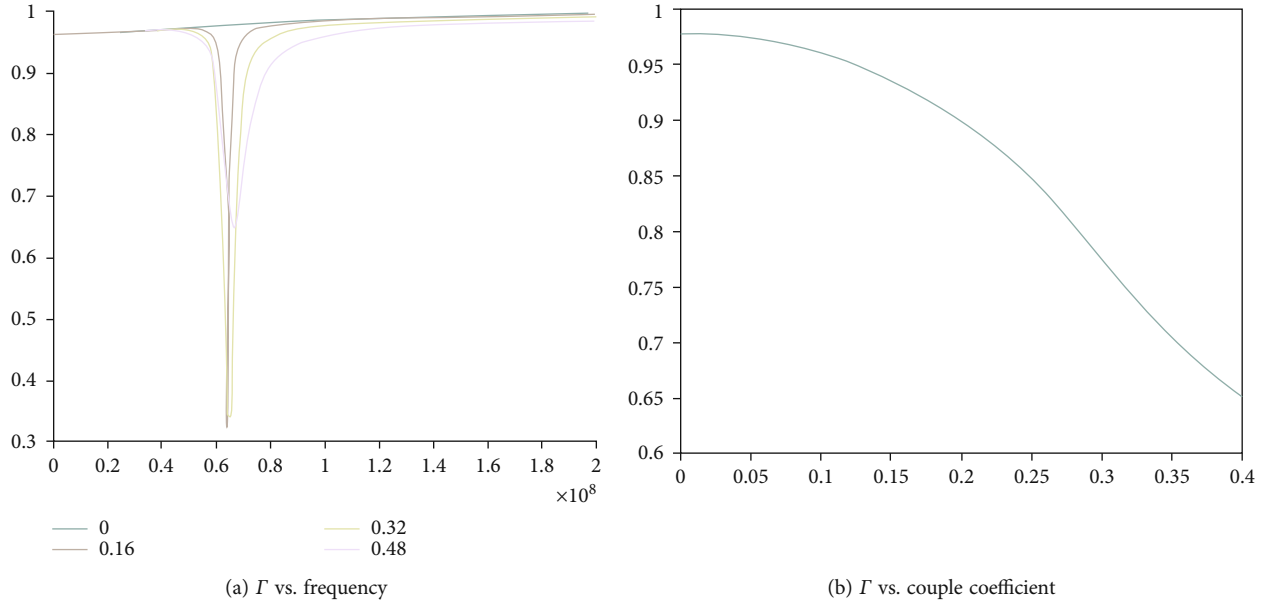

(a) Γ vs. frequency

(b) Γ vs. couple coefficient

FIGURE 2: Simulated reflection coefficient Γ versus frequency and couple coefficient, for $L_r = 100\,\text{nH}$, $R_r = 5\,\Omega$, $k = 0.25$, $f_0 = 100\,\text{MHz}$, and $Q = 8$.

readout antenna S_{11} parameter can be written as

$$S_{11} = 20\,\lg\,(\Gamma), \tag{5}$$

where lg is the logarithm function and Γ is the reflection coefficient of the readout antenna. The measured output voltage can be converted to the S_{11} parameter that represents the coupling coefficient. Owing to the relative position of the antenna to the sensor derive couple coefficient, the reflect coefficient can be used to detect the relative position and rotational speed. Table 1 presents the simulated S_{11} parameter versus lateral displacement. From the data, we can derive the lateral displacement.

The periodic rotation of the rotor causes the sensor to approach and move away from the readout antenna periodically. In a small angle range, because the sensor approximately moves in a straight line, the lateral displacement is given by

$$d = r\sin\theta \approx \theta, \tag{6}$$

where d is the lateral displacement and r is the rotor radius. If the angle is larger than 19 mm, the sensor and the readout antenna are approximately uncoupled. In [19], Zierhofer and Hochmair investigated the lateral displacement against the coupling coefficient. We calculate V_{out} from Figure 4. The point where the lateral displacement is 0 mm between
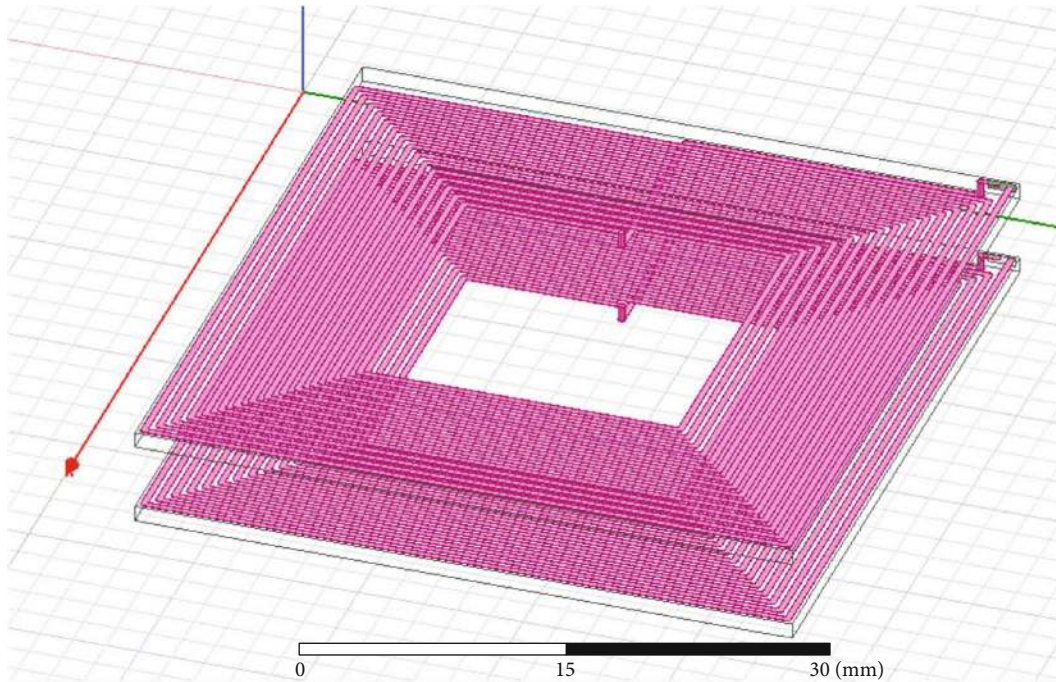
(a) Simulated model for readout antenna and sensor

Name	X	Y
m1	132.00	−9.7933

Curve info
dB (S(1,1))
HFSS_setup_1:sweep_1
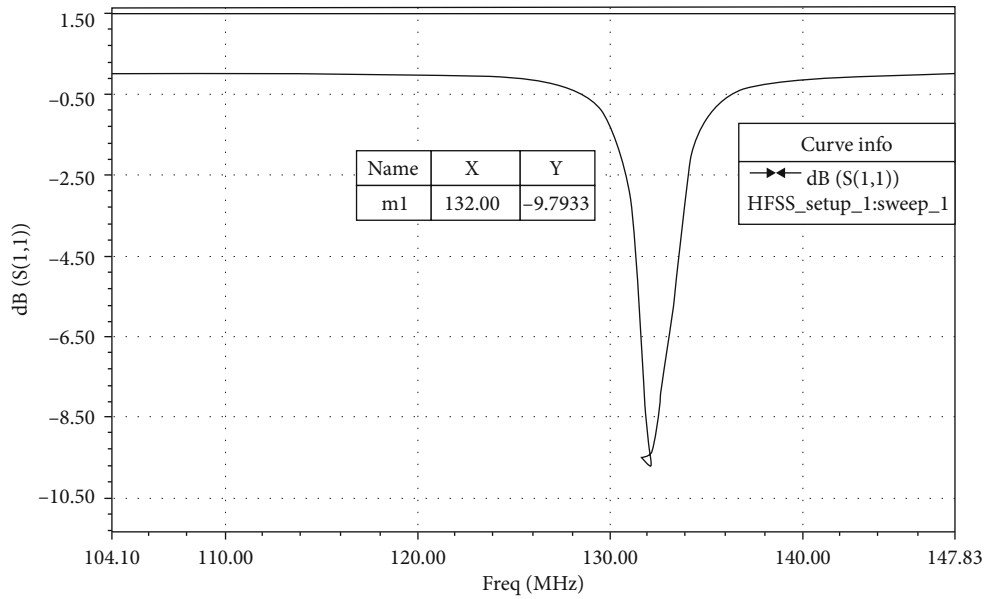
(b) Simulated S parameter of a single readout antenna

FIGURE 3: Simulated and calculated coupling coefficient versus lateral displacement between the sensor with the antenna. Both readout antenna and sensor outmost turn are $l_0 = 40$ mm.

TABLE 1: Simulated S_{11} versus lateral displacement. The reflection coefficient is calculated by equipment.

L_d	S_{11} (dB)	L_d	S_{11} (dB)	L_d	S_{11} (dB)	L_d	S_{11} (dB)
0	-13.59	5	-8.84	10	-5.80	15	-3.30
1	-12.18	6	-8.04	11	-5.50	16	-2.04
2	-10.57	7	-7.91	12	-4.30	17	-1.22
3	-9.73	8	-7.86	13	-3.54	18	-0.74
4	-9.52	9	-6.66	14	-3.52	19	-0.47

In Table 1, L_d is the lateral displacement in millimeter.

the sensor and the antenna defines the 0 degrees. Figure 4 shows the algorithm that determines the rotational speed at a constant rotational speed. Whereas the rotor is rotating, the output V_{out} changes periodically with the same frequency.

In the rotation, if the LC resonator and the antenna are directly opposite, the impedance amplitude of the antenna end reaches the minimum value, and the voltage amplitude of the read antenna terminal reaches the minimum value. Therefore, in the rotation of the object, there will be a
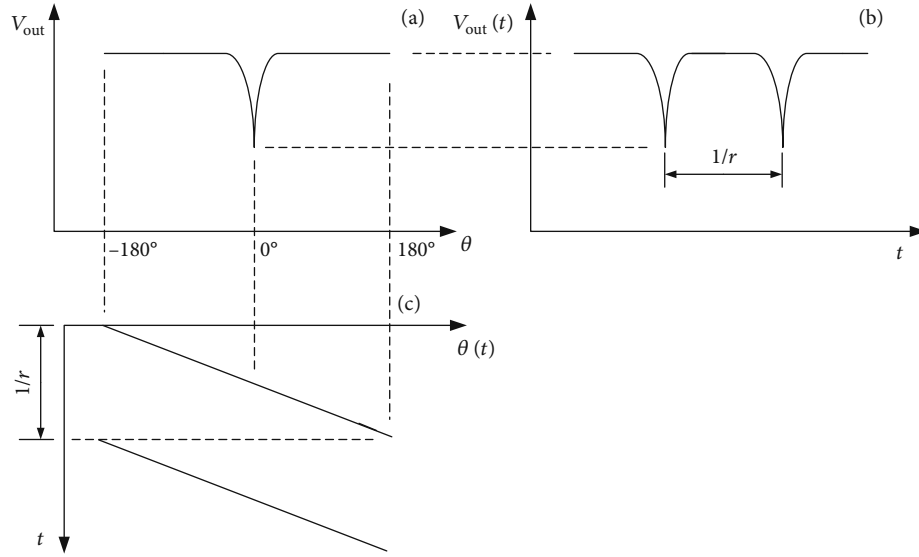
FIGURE 4: Principle of rotational speed detect algorithm (a) simulated V_{out} versus theta and (b) simulated V_{out} versus time, while the sensor is put on rotor with rotational speed of 60 r/min. (c) Theta versus time while the rotor is rotating.
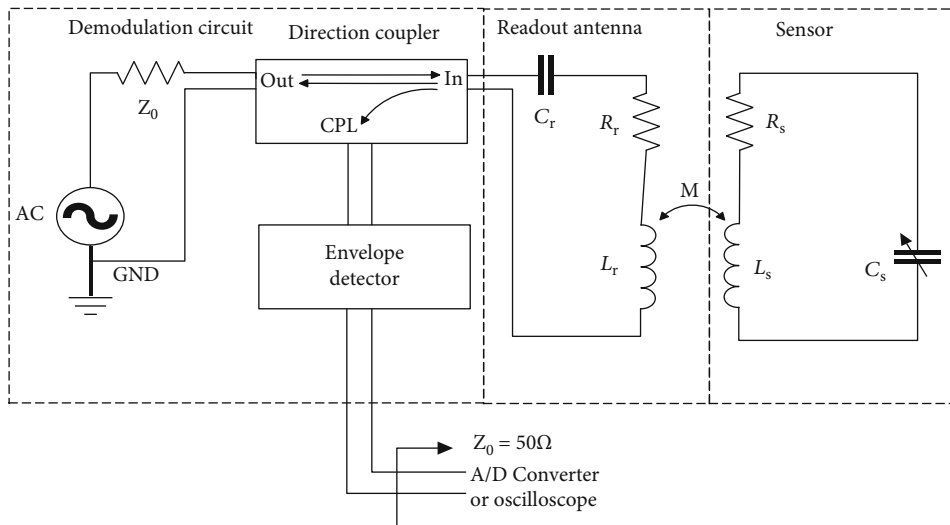

FIGURE 5: Lumped parameter circuit schematic view of the wireless rotational speed sensor system. RF signal generator generates a variable frequency signal. Directional coupler and ADC or oscilloscope collect RF reflected signal to determine the coupling coefficient. The sensor and the readout system convert the position information into a coil-coupling coefficient.

periodically changing voltage signal, and the amplitude decreases periodically, so that by tracking multiple trough points time interval to achieve the measurement of speed. Record the time of adjacent troughs as t_1 and t_2, respectively, $(t_1 - t_2)$ is the time interval between the LC resonator and the adjacent position of the reading antenna, and the rotation speed of the measured object is

$$v = \frac{1}{t_2 - t_1}. \tag{7}$$

2.3. Single Tune Readout System. Several studies have proposed detecting the sensor couple coefficient using the real part of the impedance with sweep frequency [13–15]. However, the sensor couple coefficient can be detected using a single point reflect coefficient. This method prevents the generation of scan frequency signals. Therefore, the overall system has a higher response time, and no sweep generator reduces the system's size and cost. Figure 5 shows the proposed structure. It has a PLL that generates an RF voltage signal, Vs = |Vs| sin2πft. A Texas instruments PLL atinum RF synthesizer LMX2571, with a delta-sigma fractional N. The PLL is used to generate the voltage signal. The output frequency of LMX2571 can be set through a microwire digital interface. This RF voltage signal drives the readout antenna. Whereas the impedance of the antenna device changes with the coupling condition, the reflected echo changes. Thus, the echo signal can be extracted with the directional coupler ZEDC-10-2B from Mini-Circuits. The ZEDC10-2B is a wideband, 1 to 1000 MHz, and 3-port

(a) The stimulation generator PCB
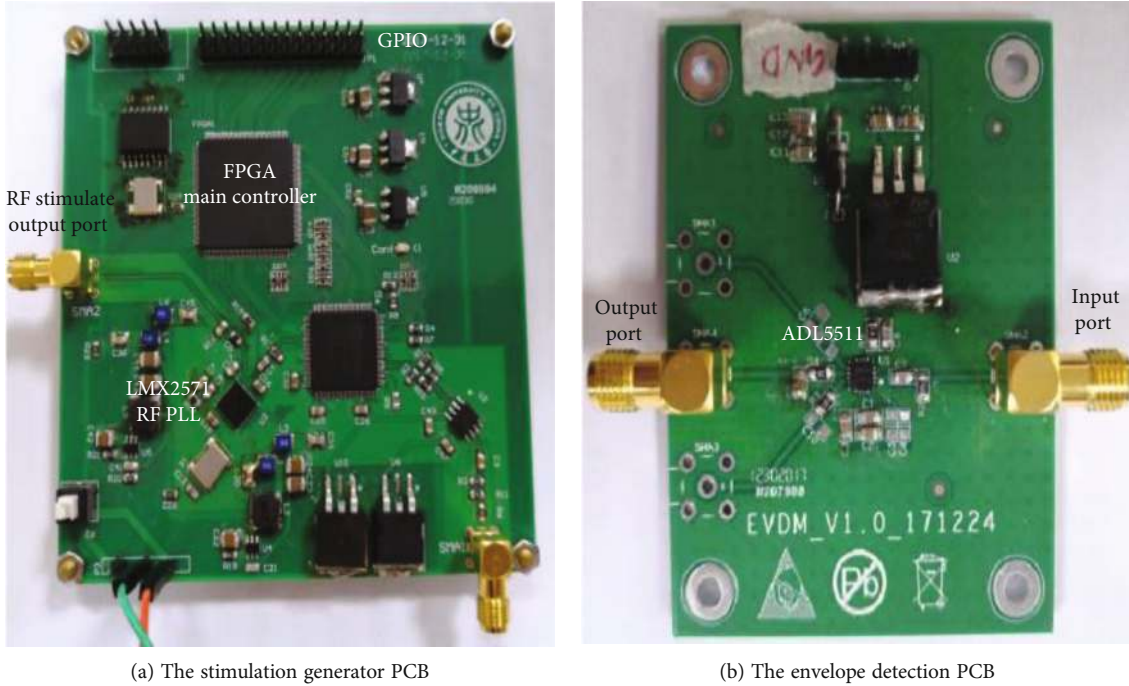

(b) The envelope detection PCB

Figure 6: Prototype of the sensor demodulating circuit. The prototype includes two PCBs: the (a) one is RF stimulation PCB, and it provides an adjustable stimulation; the (b) one is envelope detection PCB, and it is used to demodulate the reflect signal of antenna and sensor. The stimulate frequency can be adjusted by the GPIO interface, and the output stimulate voltage V_{out} is fed to the left subminiature version B (SMB) connector.

Table 2: Sensor's geometrical structure parameter.

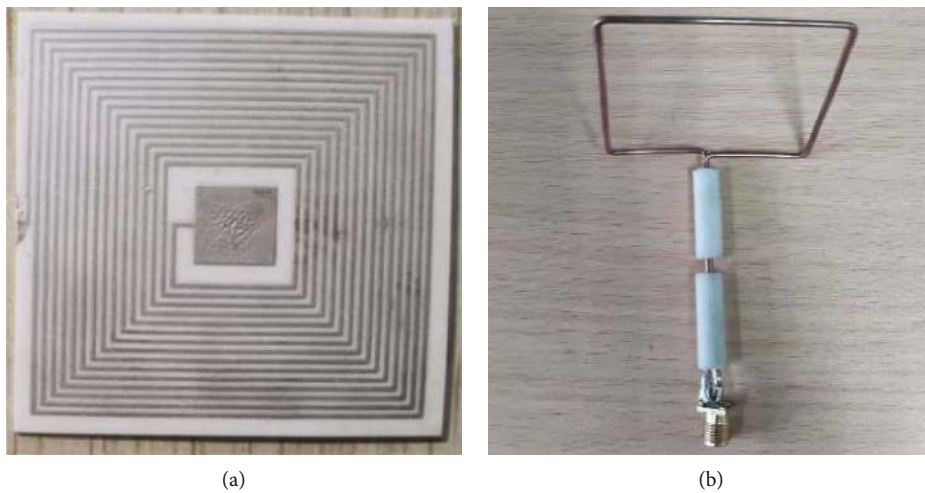| Parameter	Symbol	Value
Edge length of the outermost turn of the sensor coil	do	40.0 mm
Edge length of the intermost turn of the sensor coil	di	11.6 mm
Edge length of parallel plate capacitor	dc	6 mm
Number of coils	N	15
The thickness of the ceramic substrate	w	0.35 mm
Width of conductor	lw	0.4 mm

(a)

(b)

Figure 7: Sensor based on 95% alumina substrate. The pattern of readout antenna is consistent with the sensor and based on FR-4 substrate: (a) the figure of fabricated sensor; (b) figure of fabricated readout antenna.
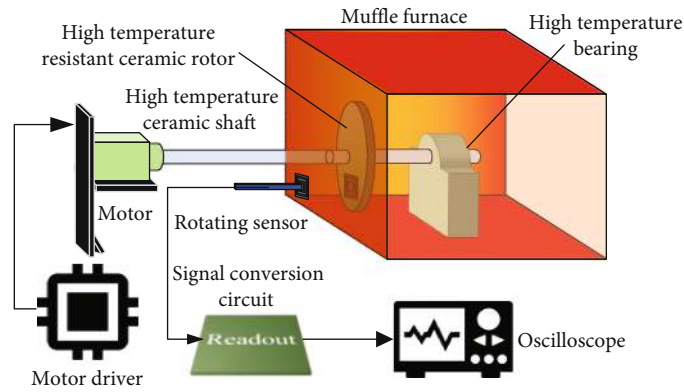
FIGURE 8: System architecture of the test bench. A high-temperature tolerance bearing is used to hold the rotating shaft made with alumina ceramic.
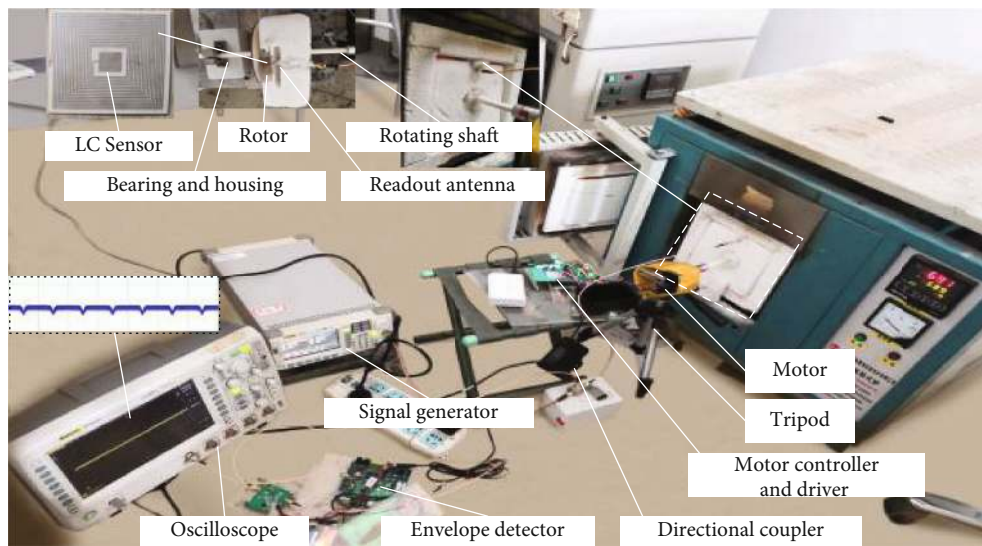

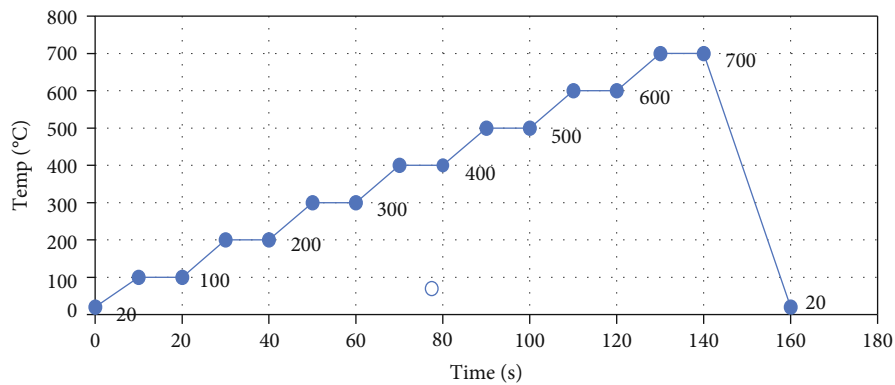FIGURE 9: The prototype of the test bench. The high-temperature environment is dominated by a BLMT-1800.

FIGURE 10: The temperature-time curve of the sensor testing.

directional coupler. The directional coupler couples the reflected echo to the coupled port. Consequently, the output of the coupled port of directional coupler is proportional to the reflection coefficient. An analog device envelope detector detects the envelope of the coupled port, and the envelope output is proportional to amplitude. The system output is

$$V_{out} = G_{env} V_{cp}, \tag{8}$$

where V_{out} is the system output and G_{env} is the conversion gain of envelope detector. In ADL5511, the normal conversion gain is 1.46 V/V. Subsequently, the envelope output
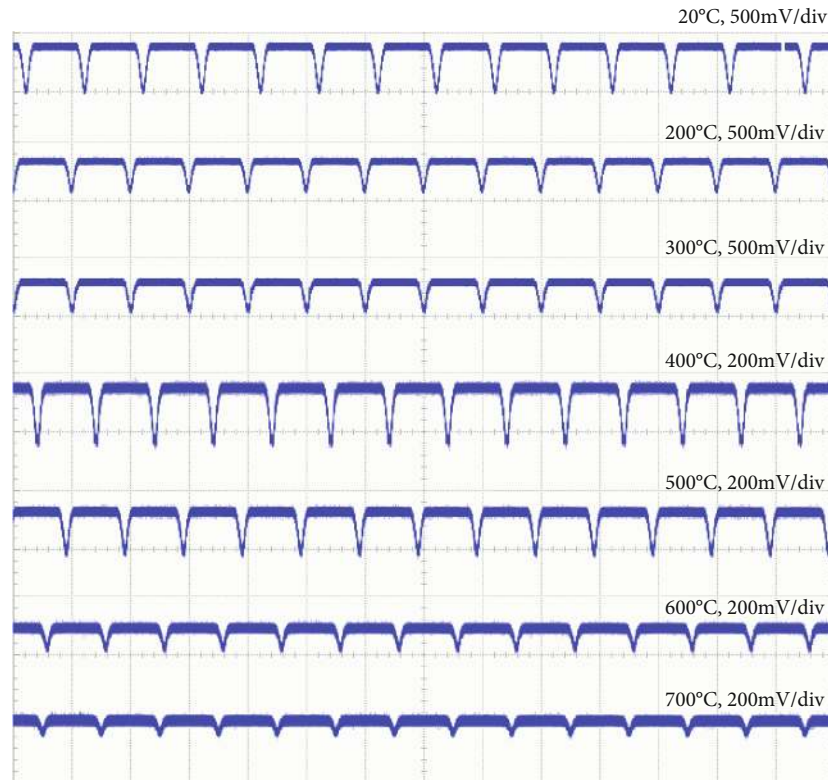
FIGURE 11: Sensor and signal conversion circuit test results. The test temperature rises one by one, from 20°C to 700°C; all curve horizontal scale is 1 s/div.
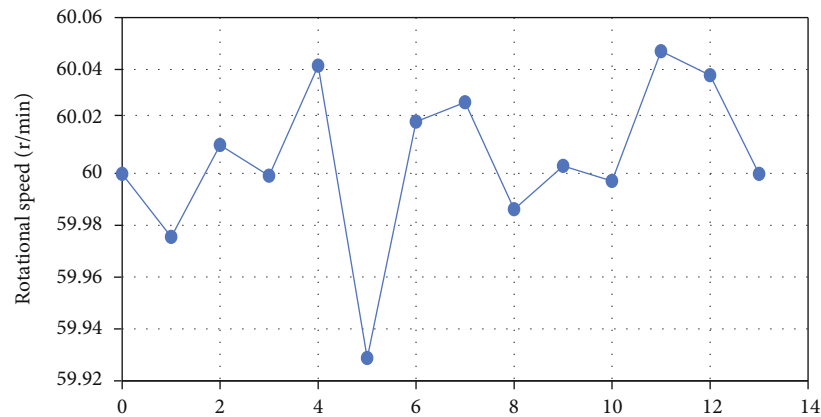

FIGURE 12: The calculated rotational speed of the sensor testing.

can be measured by analog-digital converter (ADC) or oscilloscope.

A prototype of the proposed frontend circuit is built using commercially available analog integrated circuits (ICs) on a printed circuit board. The prototype is depicted in Figure 6.

2.4. Sensor Geometrical and Fabrication. From [19], the working frequency of the sensor is closely related to the geometric size of the sensor. From the simulation, the number of coil turns has significant impact on the coil's own inductance and the sensor's quality factor. From the computations and comparisons, we determined the following structural parameters. The reasonable size of the sensor is presented in Table 2.

In standard thick film integration technology, the sensor is sintered using a 95% alumina substrate and silver paste. The top of the 1st layer and the bottom of the 3rd layer were screen printed on the silver pattern in the initial step. All layers of tape were stacked and laminated. Thereafter, the stack was placed into a box furnace and applied a high temperature to shape the sensor. An image of the fabricated sensor is shown in Figure 7.

3. Experiment and Discussion

To investigate the readout system, a rotational speed test bench was developed. Figures 8 and 9 present the full view

of the test bench. The sensor is glued to the turn plate that is held using a bearing. Thereafter, the plate is placed into the muffle furnace, and the motor is used to rotate the sensor at a constant speed.

The readout antenna is coupled with the rotating sensor at 5 mm distance. The antenna is connected to the readout system whereas the output of the readout system is connected to a rigol DS6064 oscilloscope.

Initially, the sensor resonance frequency is determined at room environment from the ANSYS electronic simulation result. Thereafter, the temperature rise curve of the muffle furnace is set based on the temperature curve from Figure 10. Each set temperature point is maintained for 10 min to measure the sensor working output. A driver is set to drive a stepper motor to rotate at a speed of 60 r/min in the entire process. We measured the output from room temperature to 700°C; the outputs are indicated in Figure 11. If the temperature ranges from 20°C to 500°C, the scales of output curve are 500 mV/div. At temperatures above 500°C, the scales of output curve are 200 mV/div. As the temperature rises, the peak of output reduces, owing to the rapid increase of the quality factor Q. The results are shown in Figure 12.

4. Conclusion

This study proposes a sensor readout system for rotational-speed measurement and uses a novel method to achieve the measurement of rotational speed at high temperatures. By introducing a sine excitation to the readout antenna, the amplitude of its reflected signal was measured to obtain the equivalent impedance. To address the weakening of signal under high temperature, we designed an amplifying circuit to address the sensitive detection problem. In addition, we developed a rotational speed-temperature composite test platform and tested the sensor using the muffle furnace. From the test, the given rotational speed signal can be measured under 700°C with an error of less than 0.12%. This depicts the effectiveness of the sensor in high-temperature environments.

Data Availability

The data used to support the findings of this study are included within the article.

Conflicts of Interest

There is no conflict of interest regarding the publication of this paper.

Acknowledgments

References

[1] C. Pan, L. Chen, L. Chen, H. Jiang, Z. Li, and S. Wang, "Research on motor rotational speed measurement in regenerative braking system of electric vehicle," *Mechanical Systems and Signal Processing*, vol. 66-67, pp. 829–839, 2016.

[2] L. Wang, Y. Yan, and K. Reda, "Comparison of single and double electrostatic sensors for rotational speed measurement," *Sensors and Actuators A: Physical*, vol. 266, pp. 46–55, 2017.

[3] C. Chen, T. Ma, H. Jin, Y. Wu, Z. Hou, and F. Li, "Torque and rotational speed sensor based on resistance and capacitive grating for rotational shaft of mechanical systems," *Mechanical Systems and Signal Processing*, vol. 142, article 106737, 2020.

[4] Z. Xie, J. Dong, Y. Li et al., "Triboelectric rotational speed sensor integrated into a bearing: a solid step to industrial application," *Extreme Mechanics Letters*, vol. 34, article 100595, 2020.

[5] L. Wang, Y. Yan, Y. Hu, and X. Qian, "Rotational speed measurement through electrostatic sensing and correlation signal processing," *IEEE Transactions on Instrumentation and Measurement*, vol. 63, no. 5, pp. 1190–1199, 2014.

[6] C. Giebeler, D. Adelerhof, A. Kuiper, J. B. A. van Zon, D. Oelgeschläger, and G. Schulz, "Robust GMR sensors for angle detection and rotation speed sensing," *Sensors and Actuators A: Physical*, vol. 91, no. 1-2, pp. 16–20, 2001.

[7] H. Huang, W. Chou, and Z. Zhang, "A high-performance angular speed measurement method based on adaptive hysteresis switching techniques," *Mechanical Systems and Signal Processing*, vol. 64-65, pp. 282–295, 2015.

[8] L. Li, H. Hu, Y. Qin, and K. Tang, "Digital approach to rotational speed measurement using an electrostatic sensor," *Sensors*, vol. 19, no. 11, p. 2540, 2019.

[9] H. Tani, D. OKISHIO, R. Lu, S. Koganezawa, and N. Tagawa, "Development of tribocharge rotational speed sensor for rolling bearing," in *The Proceedings of the Conference on Information, Intelligence and Precision Equipment: IIP*, vol. 2018, Japan, 2018.

[10] H. Lin and K. Ding, "A new method for measuring engine rotational speed based on the vibration and discrete spectrum correction technique," *Measurement*, vol. 46, no. 7, pp. 2056–2064, 2013.

[11] Ł. Kędzierski, "High speed imaging method for rotational speed calibration," *Przegląd Elektrotechniczny*, vol. 1, no. 5, pp. 186–189, 2019.

[12] T. Wang, Y. Yan, L. Wang, Y. Hu, and S. Zhang, "Instantaneous rotational speed measurement using image correlation and periodicity determination algorithms," *IEEE Transactions on Instrumentation and Measurement*, vol. 69, no. 6, pp. 2924–2931, 2020.

[13] K. Gintner, "Rotational Speed Sensor for High Temperature," in *18. Internationales Stuttgarter Symposium*, M. Bargende, H.-C. Reuss, and J. Wiedemann, Eds., pp. 761–772, Springer Fachmedien Wiesbaden, Wiesbaden, 2018.

[14] C. Li, Q. Tan, P. Jia et al., "Review of research status and development trends of wireless passive LC resonant sensors for harsh environments," *Sensors*, vol. 15, no. 6, pp. 13097–13109, 2015.

[15] M. Sun, Y.-Q. Zhang, Y.-X. Guo, M. F. Karim, O. L. Chuen, and M. S. Leong, "Integration of circular polarized array and lna in LTCC as a 60-GHz active receiving antenna," *IEEE Transactions on Antennas and Propagation*, vol. 59, no. 8, pp. 3083–3089, 2011.

[16] C. Li, Q. Tan, C. Xue, W. Zhang, Y. Li, and J. Xiong, "A high-performance LC wireless passive pressure sensor fabricated using low-temperature co-fired ceramic (LTCC) technology," *Sensors*, vol. 14, no. 12, pp. 23337–23347, 2014.

[17] R. Nopper, R. Has, and L. Reindl, "A wireless sensor readout system—circuit concept, simulation, and accuracy," *IEEE Transactions on Instrumentation and Measurement*, vol. 60, no. 8, pp. 2976–2983, 2011.

[18] B. Wang, M.-K. Law, J. Yi, C.-Y. Tsui, and A. Bermak, "A -12.3 DBm UHF passive RFID sense tag for grid thermal monitoring," *IEEE Transactions on Industrial Electronics*, vol. 66, no. 11, pp. 8811–8820, 2019.

[19] J. Hannula and V. Viikari, "Uncertainty analysis of intermodulation based antenna measurements," in *2016 10th European Conference on Antennas and Propagation (EuCAP)*, pp. 1–5, Davos, Switzerland, 2016.

[20] C. M. Zierhofer and E. S. Hochmair, "Geometric approach for coupling enhancement of magnetically coupled coils," *IEEE Transactions on Biomedical Engineering*, vol. 43, no. 7, pp. 708–714, 1996.